

REVISED DIAGNOSTIC DIAGRAMS FOR PLANETARY NEBULAE

H. Riesgo and J. A. López

Instituto de Astronomía
Universidad Nacional Autónoma de México, Ensenada, B. C., México

Received 2005 September 28; accepted 2005 November 15

RESUMEN

Se presentan diagramas de diagnóstico de densidad electrónica-excitación para una muestra de 613 nebulosas planetarias. En base a esta extensa muestra se definen nuevos límites estadísticos para la distribución de nebulosas planetarias en los planos $\log [\text{H}\alpha/[\text{S II}]]$ versus $\log [\text{H}\alpha/[\text{N II}]]$, $\log [\text{H}\alpha/[\text{S II}]]$ versus $[\text{S II}] \lambda\lambda 6717/6731$ y $\log [\text{H}\alpha/[\text{N II}]]$ versus $[\text{S II}] \lambda\lambda 6717/6731$. Los diagramas proveen una buena representación de los intervalos de condiciones físicas, indicados por estos cocientes de líneas de emisión, presentes en nebulosas planetarias en diferentes estados de evolución.

ABSTRACT

Diagnostic diagrams of electron density-excitation for a sample of 613 planetary nebulae are presented. The present extensive sample allows the definition of new statistical limits for the distribution of planetary nebulae in the $\log [\text{H}\alpha/[\text{S II}]]$ versus $\log [\text{H}\alpha/[\text{N II}]]$, $\log [\text{H}\alpha/[\text{S II}]]$ versus $[\text{S II}] \lambda\lambda 6717/6731$, and $\log [\text{H}\alpha/[\text{N II}]]$ versus $[\text{S II}] \lambda\lambda 6717/6731$ planes. The diagrams provide a good representation of the ranges of physical conditions, indicated by these emission line ratios, present in planetary nebulae during different evolutionary stages.

Key Words: ISM: PLANETARY NEBULAE

1. INTRODUCTION

Plots of emission line ratios provide useful diagnostics of the physical conditions and identification of classes of ionized gaseous nebulae. Electron density-excitation diagrams were introduced by Sabbadin, Minello, & Bianchini (1977), SMB77 hereafter, with the specific purpose of clarifying the nature of the nebula S 176. These diagrams compare the relative line intensities of the $\text{H}\alpha/[\text{N II}]$, $[\text{S II}] \lambda\lambda 6717/6731$, and $\text{H}\alpha/[\text{S II}]$ ratios observed in supernova remnants, planetary nebulae (PNe) and H II regions. These nebulae are expected to occupy distinct regions in the diagrams as a consequence of the different physical processes operating within them. For example, supernova remnants are mainly shock excited nebulae, where low $\text{H}\alpha/[\text{N II}]$ and $\text{H}\alpha/[\text{S II}]$ ratios are expected across a range of electron densities. H II regions are photoionized nebulae that show a restricted range of excitation conditions and electron densities in their generally diluted environments. Meanwhile, planetary nebulae show a wide range of excitation conditions and electron densities

depending upon their evolutionary stage, the possible presence of collimated outflows and shocks and the progenitor mass, that may influence the observed $\text{H}\alpha/[\text{N II}]$ ratio.

Recently, Phillips (2004) has discussed the distribution and significance of other relevant emission line ratios in PNe. Emission line ratio plots have also been used to distinguish planetary from symbiotic nebulae (e.g., Gutiérrez Moreno, Moreno, & Cortéz 1995). The SMB77 diagrams have proven to be a useful diagnostic tool for PNe and have been used widely in a number of works (e.g., Barral et al. 1982; López & Meaburn 1983; García Lario et al. 1991; Tajitsu et al. 1999). In the case of PNe the data in these diagrams often fall outside the original boundaries fit by SMB77, most likely as a consequence of the limited sample available then to set the diagram limits. The information used originally by SMB77 to define the parameter space for the PNe was obtained from the limited compilation made by Kaler (1976), where relative emission line intensities observed in planetary and diffuse nebulae are listed from differ-

ent sources. The estimated available number of PNe with the required information in that catalogue is of only about 40 objects. The information for H II regions in SMB77 was also obtained from that same source, whereas the data for Supernova remnants was taken from Daltabuit, D’Odorico, & Sabbadin (1976), Sabbadin & D’Odorico (1976), and Dopita (1976).

Here we have taken advantage of line intensities listed in the Strasbourg Catalogue of Galactic Planetary Nebulae, part II, SCGPN II hereafter, (Acker et al. 1992) to explore the empirical location of PNe in the SMB77 diagrams, but now based upon a much larger and homogeneous sample.

2. THE SAMPLE

In order to update the parameter intervals of the $\log [H\alpha/[N II]]$, $[S II] \lambda\lambda 6717/6731$, and $\log [H\alpha/[S II]]$ line ratios for PNe, we have compiled a database with 613 objects from the SCGPN II that provide the line intensities required in the diagrams.

The $H\alpha/[N II]$ ratio involves both $[N II]$ lines, namely $\lambda 6548$ and $\lambda 6584$, whereas the SCGPN II provides only data for the stronger $\lambda 6584$ line. We have included the contribution from the $\lambda 6548$ line by assuming a typical ratio $\lambda 6584/\lambda 6548 = 2.94$.

Figures 1, 2, and 3 show the distribution of the present dataset compared with the original zones for PNe, H II Regions and SNR as proposed by SMB77. The present sample requires an expansion of the original axes limits. Fig. 1 shows the $\log [H\alpha/[S II]]$ versus $\log [H\alpha/[N II]]$ intensity ratios; Fig. 2 the $\log [H\alpha/[S II]]$ versus $[S II] \lambda\lambda 6717/6731$ ratios, and Fig. 3 the $\log [H\alpha/[N II]]$ versus $[S II] \lambda\lambda 6717/6731$ ratios. In Figs. 2 and 3 we have added dashed horizontal lines that indicate the range for which the $[S II]$ intensity ratio is a reliable indicator of the electron density (Osterbrock 1974). The corresponding electron density scales are included on the right axes of these figures. Fig. 1 and Figure 4 contain the 613 objects in our sample; Fig. 2 and 3, and Figure 5 and Figure 6, that involve the $[S II] \lambda\lambda 6717/6731$ ratio contain only 550 objects for there were 52 objects with only one $[S II]$ line listed in the SCGPN II which precluded obtaining the $[S II]$ line ratio. Likewise, eleven additional objects were also discarded in those diagrams for having an unlikely large $[S II] \lambda\lambda 6717/6731 > 2$.

3. DISCUSSION

It is clear from Figs. 1 through 3 that the limits and zones defined for PNe in the original sample used by SMB77 fall short of covering substantial data regions in these diagrams. The present extended

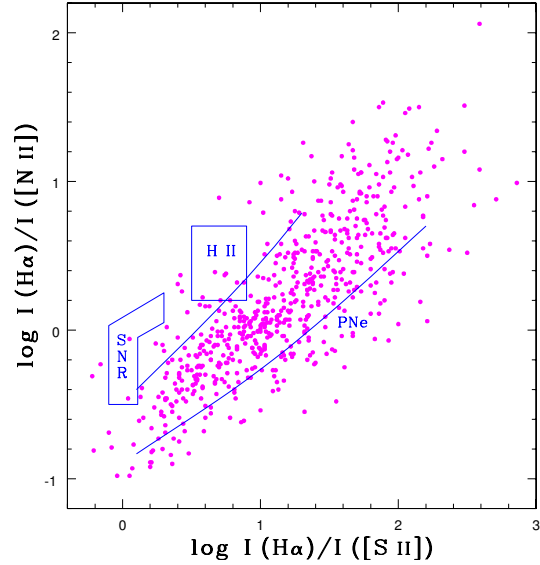


Fig. 1. The database used in this work is plotted in the $\log [H\alpha/[S II]]$ versus $\log [H\alpha/[N II]]$ plane. The original zones for SNR, H II regions and PNe proposed by SMB77 are indicated.

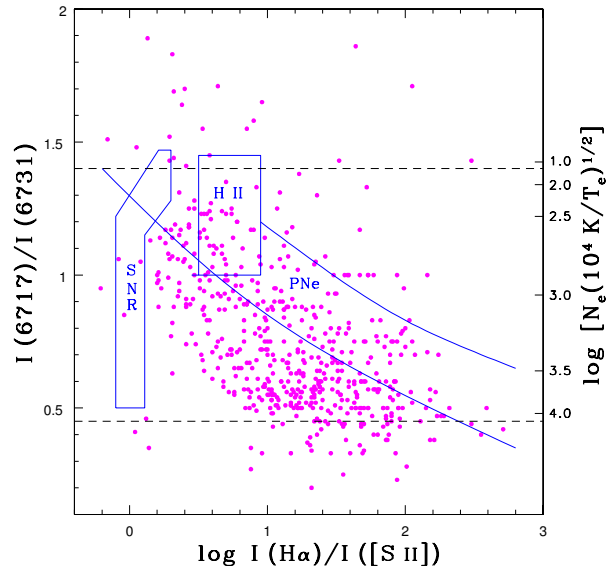


Fig. 2. As in Figure 1, but for the $\log [H\alpha/[S II]]$ versus $[S II] \lambda\lambda 6717/6731$ plane. The horizontal dashed lines indicate the range of values for which the $[S II] \lambda\lambda 6717/6731$ ratio is a valid indicator of the electron density.

sample from the SCGPN II expands the previous location of PNe in the diagrams, providing a more accurate representation of their zones of influence.

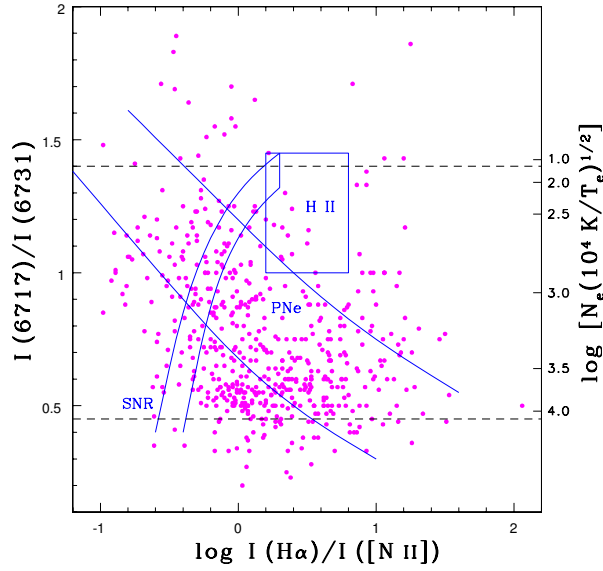


Fig. 3. As in Figure 1, but for the $\log [H\alpha]/[N II]$ versus $[S II]$ $\lambda\lambda 6717/6731$ plane. The horizontal dashed lines indicate the range of values for which the $[S II]$ $\lambda\lambda 6717/6731$ ratio is a valid indicator of the electron density.

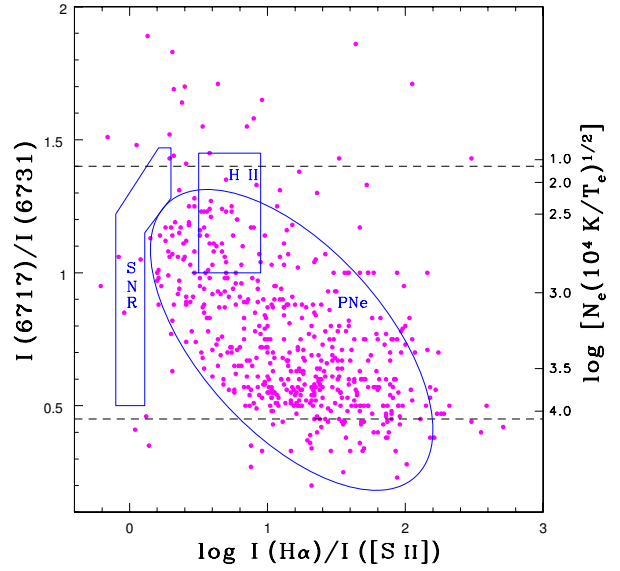


Fig. 5. As in Figure 4, but for the $\log [H\alpha]/[S II]$ versus $[S II]$ $\lambda\lambda 6717/6731$ plane. The correlation coefficient is -0.58 .

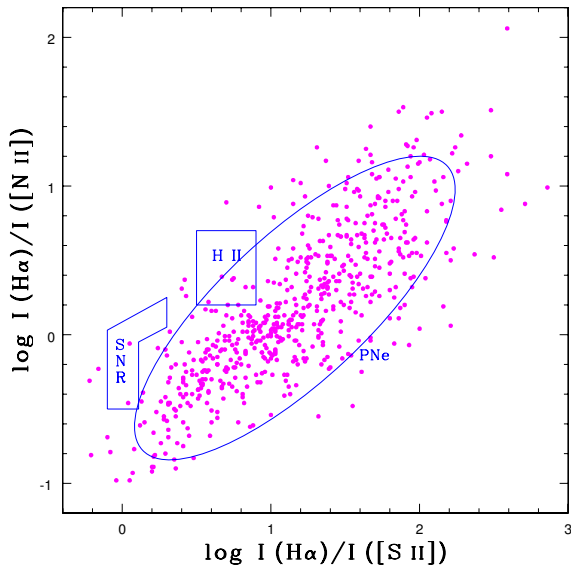


Fig. 4. Diagnostic diagram for the $\log [H\alpha]/[S II]$ intensity ratio versus $\log [H\alpha]/[N II]$ ratio with the new limits defined by a density ellipse of probability 0.85. The correlation coefficient is 0.79.

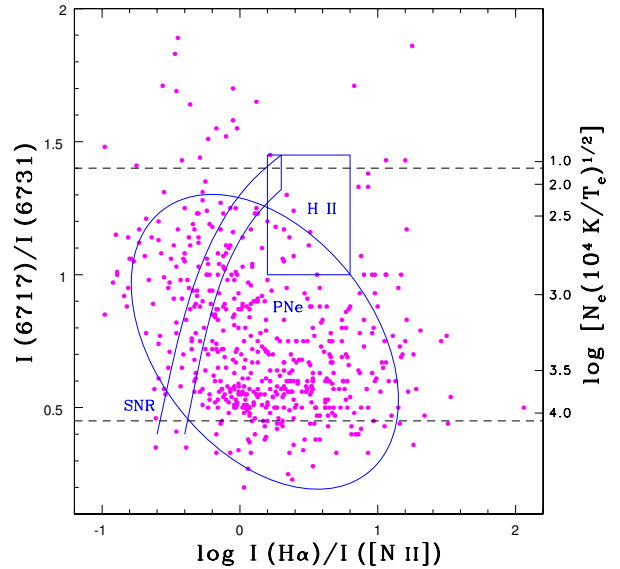


Fig. 6. As in Figure 4, but for the $\log [H\alpha]/[N II]$ versus $[S II]$ $\lambda\lambda 6717/6731$ plane. The correlation coefficient is -0.37 .

New statistical limits therefore have now been set to represent the location of PNe in the SMB77 diagrams by means of density ellipsoid probabilities. Figs. 4, 5, and 6 show the new zones defined

by ellipses of probability 0.85 for the corresponding emission line ratios for PNe. The ellipse in the diagrams represents both the density contour and confidence region of finding an object within this zone

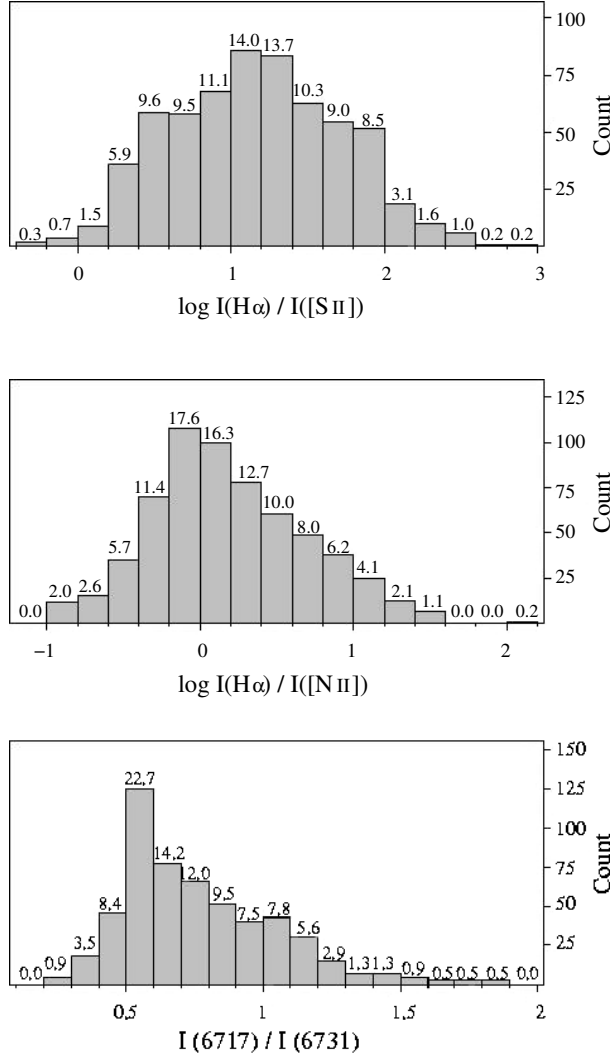


Fig. 7. Histograms of the distribution of the values for the corresponding line ratios. Numbers at the top of each bar correspond to the percentage value of that column in relation to the total sample.

with an 85% confidence level. The density ellipse is also a good graphical indicator of the correlation between the two variables involved. The ellipse collapses across its minor axis, i.e., becomes thinner, as the correlation between the two variables increases and approaches unity (± 1) and expands or reduces its eccentricity as the correlation weakens. The density ellipses in Figs. 4, 5, and 6 have all been set for a 0.85 probability; however the correlation coefficients differ among them, with values of 0.79, -0.58 and -0.37 , respectively. Thus, the correlation between $\log [H\alpha/[S II]]$ versus $\log [H\alpha/[N II]]$ is strongest, whereas that between $\log [H\alpha/[N II]]$ versus $[S II] \lambda\lambda 6717/6731$ is weakest. The correlation is

related to the scatter of the points in the diagrams and this scatter is a combination of a real dispersion due to different physical conditions, as those expected from different evolutionary stages of a planetary nebula, different conditions within a nebula (e.g., core, rim or halo) and, in some cases, also probable observational uncertainties or measuring errors from the spectroscopic SCGPN II survey. Phillips (2004) has discussed a number of factors that potentially affect such samples, such as the aperture (slit) size and its location over the nebula.

The samples for each diagram follow the trends apparent in the original SMB77 diagrams, though now they cover zones where the concentration and correlation of the line ratios provide a much closer representation of the true location of PNe in these diagnostic diagrams. For example, the ellipses in Figs. 5 and 6 show a clear tendency towards larger electron density values as compared to the corresponding original areas indicated in Figs. 3 and 4. These values are in good accord with the electron densities derived from other, smaller, samples such as in Stanghellini & Kaler (1989).

The diagrams provide direct and useful information on general physical conditions in PNe. For example, diluted shells with low electron density and low to moderate excitation conditions, e.g., $0.5 < \log [H\alpha/[S II]] < 1$ (see Fig. 5) will overlap the location of H II regions. These objects are likely large, evolved PNe. The likely presence of shock contributions in the dominantly photoionized environment of PNe is hinted at by objects located in Fig. 4 in the $\log [H\alpha/[N II]] < 0$ and $\log [H\alpha/[S II]] < 0.4$ region. Objects with high electron density and high $H\alpha$ emissivity in Figs. 5 and 6 point towards compact, young PNe. For PNe for which limited information is available, their location on the diagrams usually provides insight into their general (or peculiar) characteristics and evolutionary stage.

Figure 7 shows the histograms of the distribution of values for the corresponding line ratios. The numbers at the top of each bar indicate the percentage of objects in the sample associated with that value in relation to the entire sample. The line ratios of PNe are concentrated around a value of 1.2 for $\log [H\alpha/[S II]]$ with a fairly even distribution on either side from the peak. For the $\log [H\alpha/[N II]]$ line ratio the values concentrate around 0.0 but fall rapidly towards negative values. Finally, the distribution of values for the $[S II] \lambda\lambda 6717/6731$ line ratio is markedly asymmetric, peaking sharply at a value of 0.6, with a smooth drop towards larger values and an abrupt fall on the other side (high density). These

values can be considered as representative for the most common or typical conditions in galactic PNe.

4. CONCLUSIONS

Values of $H\alpha/[N II]$, $[S II] \lambda\lambda 6717/6731$, and $H\alpha/[S II]$ for 613 planetary nebulae have been derived from the Strasbourg Catalogue of Planetary Nebulae, part II (Acker et al. 1992) and plotted in the Sabbadin et al. (1977) diagnostics diagrams. The current sample substantially expands the sample used in the original diagrams and allows a redefinition of the parameter space of PNe in the $\log [H\alpha/[S II]]$ versus $\log [H\alpha/[N II]]$, $\log [H\alpha/[S II]]$ versus $[S II] \lambda\lambda 6717/6731$, and $\log [H\alpha/[N II]]$ versus $[S II] \lambda\lambda 6717/6731$ planes. Accordingly, new statistical limits have been set for the location of PNe in these diagrams using density ellipses of probability 0.85. We find a good, 0.79 correlation for the $\log [H\alpha/[S II]]$ versus $\log [H\alpha/[N II]]$ intensity ratio; a modest -0.58 correlation for the $\log [H\alpha/[S II]]$ versus $\log [H\alpha/[N II]]$ intensity ratio and a poor, -0.37 correlation in the case of $\log [H\alpha/[N II]]$ versus $[S II] \lambda\lambda 6717/6731$. From our study we obtain the statistical distribution of emission line ratios expected in PNe. These upgraded diagnostic diagrams provide a better representation of the ranges of physical conditions indicated from the emission line ratios and allow the identification and study of groups or individual PNe of particular interest in specific regions of the diagrams.

Finally, in relation to the parameter space for the H II and SNR regions, the data sources in SMB77 for these two cases were restricted to a limited number of objects, as in the original case for PNe. For the H II regions the compilation made by Kaler (1976) was used. For the supernovae the data is based on 17 galactic remnants. It would be clearly useful to revise and update the parameter space for the H II and

SNR regions so as to assess the reliability of their distributions in the revised diagrams. This is presently out of the scope of the present paper but worth pursuing as a natural extension of this work.

Templates in poscript or pdf format of the revised diagrams, Figs. 4, 5, and 6, are available from J. A. López.

HR acknowledges a posgraduate scholarship from CONACYT. JAL acknowledges continued support from DGAPA-UNAM and CONACYT through grants IN112103 and 43121, respectively. We thank M. Richer and W. Steffen for their comments on this work and the anonymous referee for helping us to improve the presentation of the paper.

REFERENCES

- Acker, A., Ochsenbein, F., Stenholm, B., Tylenda, R., Marcout, J., & Schohn, C. 1992, Strasbourg-ESO Catalogue of Galactic Planetary Nebulae, ESO
- Barral, J. F., Cantó, J., Meaburn, J., & Walsh, J. R. 1982, MNRAS, 199, 817
- Daltabuit, E., D'Odorico, S., & Sabbadin, F. 1976, A&A, 52, 93
- Dopita, M., A. 1976, ApJ, 209 395
- García-Lario, P., Manchado, A., Riera, A., Mampaso, A., & Pottasch, S. 1991, A&A, 249, 223
- Gutiérrez-Moreno, A., Moreno, H., & Cortés, G. 1995, PASP, 107, 462
- Kaler, J. B. 1976, ApJS, 31, 517
- López, J.A. & Meaburn, J. 1983, MNRAS, 204, 203
- Osterbrock, D. E. 1974, Astrophysics of Gaseous Nebulae (San Francisco: W. H. Freeman and Co.)
- Phillips, J. P. 2004, RevMexAA, 40, 193
- Sabbadin, F., & D'Odorico, S. 1976, A&A, 49, 119
- Sabbadin, F., Minello, S., & Bianchini, A. 1977, A&A, 60, 147
- Stanghellini, L., & Kaler, J. B. 1989, ApJ, 343 811
- Tajitsu, A., Tamura, S. Yadoumaru, Y., Weinberger, R., & Koppen, J. 1999, PASP, 111, 1157